Numerical unfoldings of codimension-three resonant homoclinic flip bifurcations

Bart E Oldeman†, Bernd Krauskopf‡ and Alan R Champneys§
Department of Engineering Mathematics, University of Bristol, Bristol BS8 1TR, UK.

Abstract. Resonant homoclinic flip bifurcations are codimension-three phenomena that act as organising centres for codimension-two inclination flip, orbit flip and eigenvalue-resonance bifurcations for homoclinic orbits to a real saddle. In a recent paper by Homburg and Krauskopf unfoldings for several cases of resonant homoclinic flip bifurcations were proposed as bifurcation diagrams on a sphere around the central singularity.

This paper presents a comprehensive numerical investigation into these unfoldings in a specific three-dimensional vector field, which was constructed by Sandstede to explicitly contain inclination flip and orbit flip bifurcations. For both orbit and inclination flips different cases can be classified according to the eigenvalues of the saddle point. All possible cases are treated including complicated ones involving homoclinic-doubling cascades and chaos. In each case, by choosing a sufficiently small sphere around the codimension-three point in parameter space, the conjectured unfoldings are largely confirmed. However, for larger spheres interesting new codimension-three bifurcations occur, leading to a more complicated bifurcation structure. The results suggest an important trade-off between finding bifurcation curves numerically and introducing new bifurcations by enlarging the sphere too much.

†E-mail: Bart.Oldeman@bristol.ac.uk, tel: +44-(0)117-9289798, fax: +44-(0)117-9251154, corresponding author.
‡E-mail: B.Krauskopf@bristol.ac.uk
§E-mail: A.R.Champneys@bristol.ac.uk

AMS classification scheme numbers: 34C37 37G15 37G20 37M20 65P30

Applied Nonlinear Mathematics Research Report 2000.7
University of Bristol, June 2000

Submitted to: *Nonlinearity*

1. Introduction

Homoclinic orbits are of importance in many applications, in fields as diverse as mathematical biology, chemistry, fluid mechanics, electronics and probability theory (Gaspard et al. 1993, Kuznetsov 1998, Koper 1995). They generically occur as a codimension-one phenomenon, in which a limit cycle becomes a homoclinic orbit and then disappears as one parameter changes. A homoclinic orbit can act as an organising centre for complicated dynamics. Best known is the case when the equilibrium that the orbit connects to itself has complex eigenvalues (a saddle-focus). Then it is possible to have chaotic behaviour involving horseshoe dynamics, as discovered by Shil'nikov (1968, 1970); see also (Guckenheimer and Holmes 1983, Kuznetsov 1998). This involves the creation of limit cycles with "infinite period", as well as n-homoclinic orbits which come close to the equilibrium for $(n-1)$ times before finishing the loop.

Here we exclusively deal with the case that the eigenvalues of the equilibrium (a saddle) are all real. In this situation there is the possibility of a homoclinic-doubling bifurcation, that is, a codimension-two transition from an n-homoclinic to a $2n$-homoclinic orbit. Homoclinic doubling in this setting has been studied since 1982, beginning with the work of Evans et al. (1982) on double impulse solutions in certain PDEs, modelling the activity of nerve-axons. The solutions of interest are travelling waves which can be studied by transforming the PDE into a system of ODEs by changing to a moving frame. Physically important solitary travelling waves or impulse solutions correspond to homoclinic orbits. Evans et al. formulated three genericity conditions for a saddle homoclinic orbit to be of codimension-one, in which case homoclinic doubling is impossible.

Yanagida (1987) pointed out that homoclinic-doubling may occur if one of the genericity conditions is violated. More recently, the different codimension-two homoclinic bifurcations allowing for homoclinic doubling have been studied in detail. The case with *resonant eigenvalues* was studied most comprehensively by Chow, Deng and Fiedler (1990). *Orbit flips*, which are non-principal homoclinic orbits, were mainly treated by Sandstede (1993). *Inclination flips*, also called critically twisted homoclinic orbits, were investigated by Homburg, Kokubu and Naudot (1997), Kisaka, Kokubu and Oka (1993*a*, 1993*b*) and Naudot (1996). For certain configurations of eigenvalues these homoclinic flip bifurcations generate chaos. See Section 2 for precise definitions.

Applications in which homoclinic doublings have been found include the FitzHugh-Nagumo nerve-axon equations (Krupa et al. 1997), a model for electro-chemical oscillators by Koper (1995), and the Shimitzu-Morioka equations (Champneys and Kuznetsov 1994, Shil'nikov 1993, Rucklidge 1993). In all these applications it is inclination flips rather than orbit flips that have been found.

When the conditions for either an orbit or an inclination flip and an eigenvalue resonance hold simultaneously, we have a codimension-three situation, called a *resonant homoclinic flip bifurcation*. These bifurcations have recently been studied by Homburg and Krauskopf (2000). They show how a homoclinic-doubling cascade (successive

homoclinic doublings), previously found to exist by Homburg et al. (1997), comes up naturally in these codimension-three unfoldings. The main aim of this paper is to use accurate numerical techniques in order to test the conjectures from Homburg and Krauskopf (2000) concerning how various codimension-two sub-cases fit together in a codimension-three sense around such an organising centre in parameter space.

The minimal dimension of phase space for these codimension-three bifurcations to occur is three, which is the dimension we restrict ourselves to. However, owing to the homoclinic center-manifold theorem (Sandstede 1999, Shashkov and Turaev 1999), the results likely apply to higher-dimensional systems as well.

All the numerical results in this paper are presented for a model proposed by Sandstede (1997), which was specifically constructed to admit all the codimension-two bifurcations under consideration here. Reasons for using this model include its complete control over all the parameters necessary to unfold the codimension-three singularities we wish to study — in a sense it is a "normal form" — and the lack of a known physical example of orbit flips other than in a Hamiltonian system (Champneys and Groves 1997). The numerics, which constitute a complete study of these bifurcations, are performed with AUTO (Doedel et al. 1997). This numerical continuation package is able, amongst many other things, to detect and follow in parameter space equilibria and periodic orbits, and related changes in the dynamics such as Hopf, period-doubling and saddle-node bifurcations. The extension HomCont(Champneys and Kuznetsov 1994, Champneys et al. 1996) can detect and follow homoclinic orbits and various codimension-two homoclinic bifurcations, including those under consideration here. For both orbit flips and inclination flips we first concentrate on a configuration of eigenvalues where only one homoclinic-doubling bifurcation is expected to occur. Secondly, a more complicated structure, involving a homoclinic-doubling cascade is investigated.

This paper is organized as follows. In Section 2 we give an overview of the theory on the codimension-one, -two and -three bifurcations that are relevant to the particular resonant homoclinic flip bifurcations treated in this paper. Section 3 then introduces Sandstede's model. Section 4 presents the results of the numerical investigation for the unfolding with only one homoclinic-doubling bifurcation. Section 5 treats the complicated case with a homoclinic-doubling cascade. Finally, Section 6 contains conclusions and an outlook to future research.

2. Overview of homoclinic bifurcations

This section gives an overview of the relevant homoclinic bifurcations that occur when one restricts to the case that the equilibrium involved has real eigenvalues. Such orbits are of codimension one provided that three non-degeneracy conditions are satisfied. Otherwise a bifurcation of codimension two or higher occurs, which can be an orbit flip or an inclination flip or a resonant bifurcation. Two cases of codimension-three bifurcation are treated here, namely the resonant orbit flip and the resonant inclination flip.

2.1. Homoclinic orbits

To be more precise, we consider bifurcations of a homoclinic orbit to a hyperbolic equilibrium in a three-dimensional vector field. The equilibrium is assumed to have two stable (negative) and one unstable (positive) eigenvalue, denoted by $-\lambda_{ss}$, $-\lambda_s$ and $\lambda_u = 1$, respectively. Note that it is always possible to scale the vector field to obtain this form. We further assume that $-\lambda_{ss} < -\lambda_s < 0$ and that the equilibrium is at the origin.

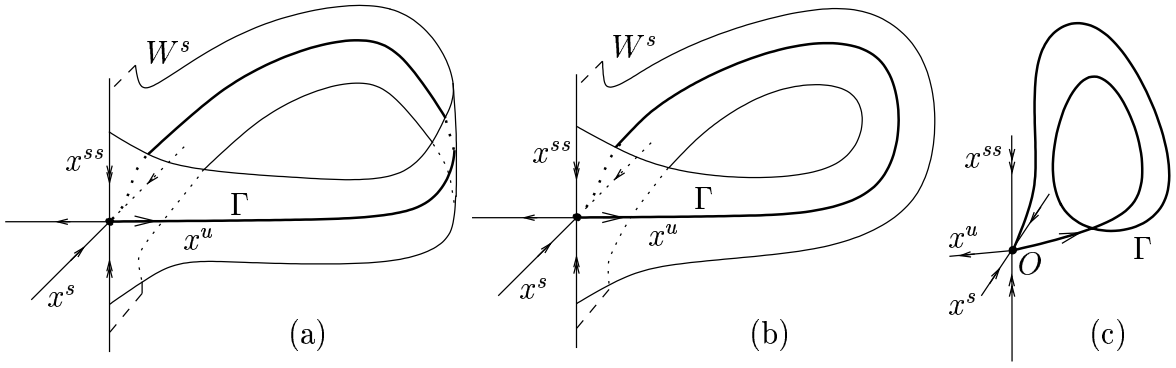

Figure 1. An orientable (a) and a twisted (b) codimension-one homoclinic orbit. A codimension-one 2-homoclinic orbit (c).

A homoclinic orbit to such a real saddle is generically of codimension-one. The genericity conditions are:

(G1) $\lambda_s \neq 1$

(G2) In positive time the homoclinic trajectory approaches the origin tangent to the weak stable direction, that is, tangent to the eigenvector associated with $-\lambda_s$.

(G3) The two-dimensional stable manifold, if followed backwards in time along the homoclinic orbit, returns to the origin along the strong stable direction. This is called the strong inclination property (Shil'nikov 1969, Deng 1989).

For a generic codimension-one homoclinic orbit there are two geometrically different possibilities: the component of the stable manifold containing the homoclinic orbit is either orientable or twisted. The two cases are depicted in Figure 1 (a) and (b), respectively. In the orientable case the stable manifold is topologically a cylinder and in the twisted case it is a Möbius strip. This distinction turns out to be crucial.

2.2. Codimension-two bifurcations

If exactly one of the above genericity conditions fails, then there is a codimension-two phenomenon, leading to the following kinds of bifurcation:

If (G1) is not satisfied, one speaks of a *resonant homoclinic orbit*, when (G2) fails of an *orbit flip*, and when (G3) fails of an *inclination flip*. The resonant

homoclinic bifurcation has been investigated by Chow et al. (1990), the orbit flip by Sandstede (1993) and the inclination flip in Kisaka et al. (1993*a*, 1993*b*) and (Naudot 1996, Homburg et al. 1997). For both an inclination flip (see Figure 2) and an orbit flip (see Figure 3) the stable manifold is neither orientable nor twisted, but is somewhere "in between". There are two different possibilities for the global organization of the stable manifold near the origin when it returns at an inclination flip homoclinic orbit, as sketched in Figure 2. This distinction depends on further eigenvalue conditions and is not important for the ensuing unfoldings. Another distinction that does matter in the unfoldings, but does not depend on the eigenvalues, is how a normal vector followed along the homoclinic orbit returns to the origin relative to the "curvature" of the stable manifold. This leads to the two cases $\mathbf{C_{in}}$ and $\mathbf{C_{out}}$ mentioned in Figure 6 described below; see also Deng (1993, Figure 2.4).

Following a homoclinic orbit through either the inclination flip or the orbit flip bifurcation changes the orientation of the stable manifold, hence the name homoclinic "flip" bifurcation. In what follows we present parameter-space bifurcation diagrams for each of these codimension-two bifurcations, in which we use the notation given in Table 1. In the notation we denote whether a homoclinic orbit is orientable or twisted. Furthermore, we show which periodic orbits are present in the open regions. This enables one to check the bifurcation diagrams for consistency.

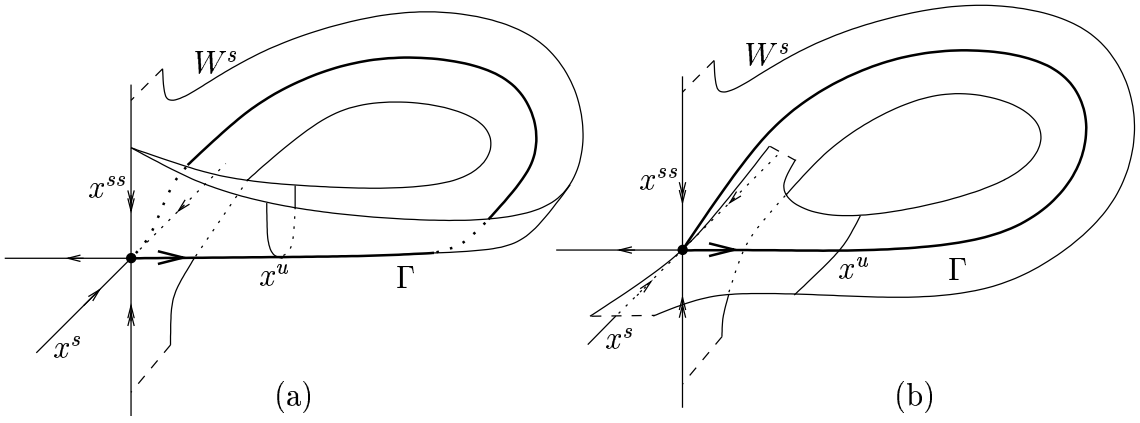

Figure 2. Codimension-two Inclination flip homoclinic orbits. Case (a) corresponds to $\lambda_{ss} > 2\lambda_s$ and case (b) corresponds to $\lambda_{ss} < 2\lambda_s$.

In all figures of codimension-two homoclinic bifurcations, the horizontal parameter η_1 breaks the resonance or the homoclinic flip bifurcation, and the vertical parameter η_2 breaks the homoclinic orbit.

For the resonant homoclinic bifurcation, there exist two cases, $\mathbf{R_o}$ and $\mathbf{R_t}$, depending on the orientation of the stable manifold. The orientable case, the *resonant side-switching bifurcation* (Chow et al. 1990) $\mathbf{R_o}$ in Figure 4 involves the birth of a saddle-node of limit cycles. If $\eta_1 > 0$, a periodic orbit bifurcates from the homoclinic orbit when η_2 is increased, whereas if $\eta_1 < 0$ this occurs when η_2 is decreased. The

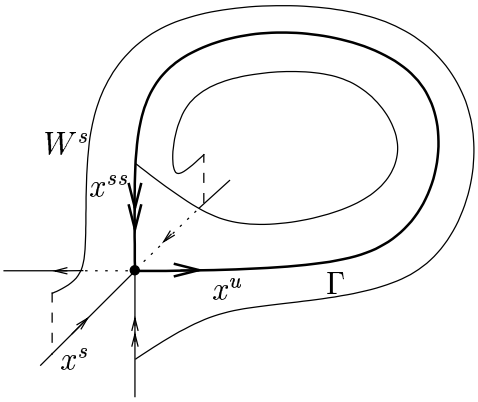

Figure 3. A codimension-two orbit flip homoclinic orbit.

Notation	Description
n^s	A *stable* n-periodic orbit exists.
n^u	An *unstable* n-periodic orbit of saddle type exists.
SN^n	A saddle-node bifurcation of n-periodic orbits.
PD^n	A period-doubling of an n-periodic orbit.
Hopf	A Hopf bifurcation.
$H^n_{t/o}$	A twisted (t) or orientable (o) n-homoclinic bifurcation.
•	All codimension-two bifurcations (such as homoclinic flips, cusp, degenerate Hopf, degenerate PD) are marked by a dot.

Table 1. The notation used in the bifurcation diagrams.

stability of this limit cycle is determined by λ_s. For $\lambda_s > 1$ the limit cycle is stable whereas for $\lambda_s < 1$ it is of saddle type. In the case $\mathbf{R_t}$ the manifold is twisted, and the bifurcation is called a *resonant homoclinic doubling* ($\mathbf{R_t}$ in Figure 4). It involves both a period doubling and a 2-homoclinic bifurcation. The 2-periodic orbit obtained from PD can be continued by increasing η_2 until it disappears in the 2-homoclinic bifurcation H^2_o. Note that we chose $\eta_1 = \lambda_s - 1$ in the unfoldings of Figure 4, which determines the stability of the limit cycles as shown.

The dynamics in a neighbourhood of an orbit flip and an inclination flip behave essentially in the same way. The key feature is that the stable manifold changes its orientation; see also Nii (1996). Depending on the eigenvalues as depicted in Figure 5, there are three cases. Note that although the three cases exist for both the inclination and the orbit flip, the eigenvalue inequalities that define them are different. The bifurcation diagrams are given in Figure 6.

A No extra bifurcations occur.

B A homoclinic-doubling bifurcation occurs. This involves the creation of a period doubling and a 2-homoclinic orbit. A saddle-node appears on the other side.

C A complicated structure involving n-periodic and n-homoclinic orbits for arbitrary

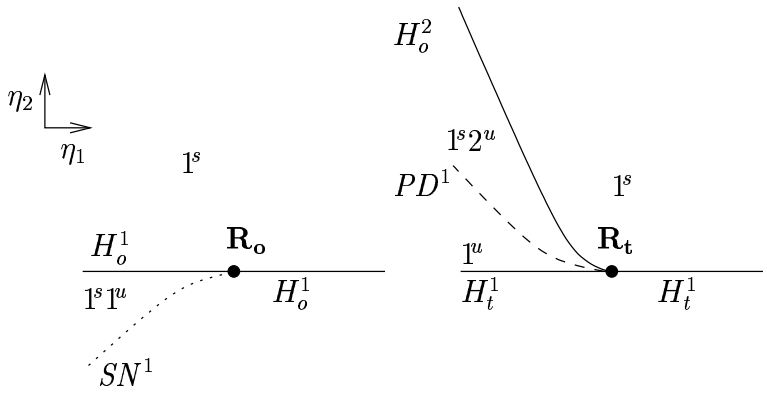

Figure 4. Possible unfoldings of the two cases $\mathbf{R_o}$ and $\mathbf{R_t}$ of resonant bifurcations: side switching $\mathbf{R_o}$ and homoclinic doubling $\mathbf{R_t}$. The resonance $\lambda_s = 1$ is broken by changing η_1. For the notation in this and all subsequent figures see Table 1.

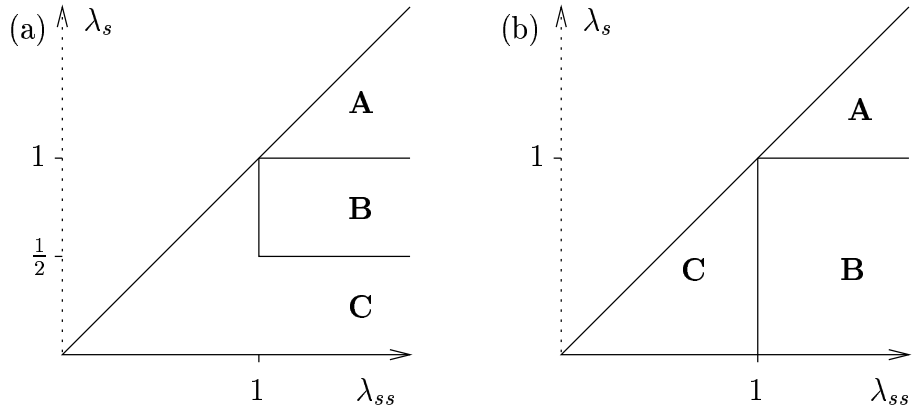

Figure 5. Eigenvalue regions for different behaviour of the inclination flip (a) and the orbit flip (b).

n and a region with horseshoe dynamics exists. Two different diagrams, $\mathbf{C_{in}}$ and $\mathbf{C_{out}}$, are possible, depending on the previously mentioned return of a vector relative to the "curvature" of the manifold, which governs how the horseshoe is created. The depicted case, $\mathbf{C_{out}}$, is the one we exclusively encounter in the numerical investigations to follow and we simply call it $\mathbf{C}$ in the sequel. For the background theory on what differentiates these two possibilities see Homburg and Krauskopf (2000) and the references stated therein.

2.3. Codimension-three bifurcations

In this section we summarize the known results and set up a basic framework for investigating the various codimension-three bifurcations. If two of the non-degeneracy conditions are not satisfied, a codimension-three bifurcation occurs. When (G1) and (G2) fail, one speaks of a *resonant inclination flip* and when (G1) and (G3) fail of a

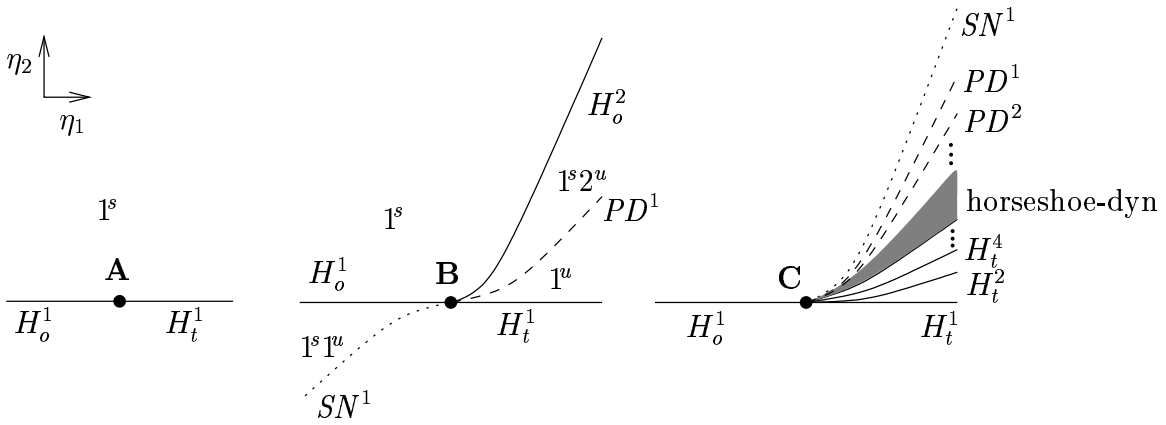

Figure 6. The different cases of homoclinic flip bifurcations. **A**: no extra bifurcations, **B**: homoclinic doubling and **C**: an infinite fan of bifurcating curves and horseshoe dynamics (the case $\mathbf{C_{out}}$ is depicted).

resonant orbit flip. These resonant flip bifurcations correspond to the border between **A** and **B** in Figure 5. However, a second degenerate homoclinic flip bifurcation occurs along the boundary between **B** and **C** in Figure 5. In what follows we refer to *both* boundaries as defining *resonant* homoclinic flip bifurcations. This corresponds to violations of eigenvalue conditions other than (G1) in combination with violation of (G2) or (G3). We do not consider the case of an *inclination orbit flip* where (G2) and (G3) are simultaneously violated.

The theory of codimension-three resonant homoclinic flip bifurcations, involving both the transition from **A** to **B** and the transition from **B** to **C**, has been developed in Homburg and Krauskopf (2000). The idea is to consider a sphere around the central codimension-three point (the organizing center) in parameter space, and to study the qualitative structure of bifurcation curves on the sphere. If this structure remains invariant under change of radius, then we say the unfolding has *cone structure* and its representation on the sphere accounts for the full dynamics.

To set the stage we consider three unfolding parameters (ν_1, ν_2, ν_3) where ν_1 and ν_2 unfold the homoclinic flip bifurcation at fixed eigenvalues and $\nu_3 = 0$ lies on a border between two eigenvalue regions. Thus for negative values of ν_3 one case of **A**, **B** or **C** occurs, whereas for positive values another case occurs, if $|\nu_3|$ is not too large.

In (ν_1, ν_2, ν_3)-space we set up the convenient spherical coordinate system

$$\begin{aligned} \nu_1 &= r \cos \pi\phi \cos \pi\theta \\ \nu_2 &= r \sin \pi\theta \\ \nu_3 &= r \sin \pi\phi \cos \pi\theta, \end{aligned} \tag{1}$$

where $\theta \in [-0.5, 0.5], \phi \in [-0.5, 1.5], r \in \mathbb{R}^+$. Clearly, (r, θ, ϕ) is parametrized by r as a family of concentric spheres. The conjecture of cone structure means that the

qualitative picture of bifurcation curves on a sphere does not change if r varies, provided it is not too large. However, if r is taken too large, other codimension-three singularities may become incorporated inside the sphere, changing the bifurcation diagram on the sphere. In all what follows, r is fixed, and θ and ϕ vary, leading to bifurcation diagrams in the (ϕ,θ)-plane, which is a "world map" representation containing all the codimension-two unfoldings around the codimension-three singularity. An example of such a representation for a possible unfolding of a transition from **A** to **B** is given in Figure 7. Other conjectured unfoldings from Homburg and Krauskopf (2000) will be discussed in the course of presenting the numerical results in Sections 4 and 5, where unless otherwise stated we refer to this article.

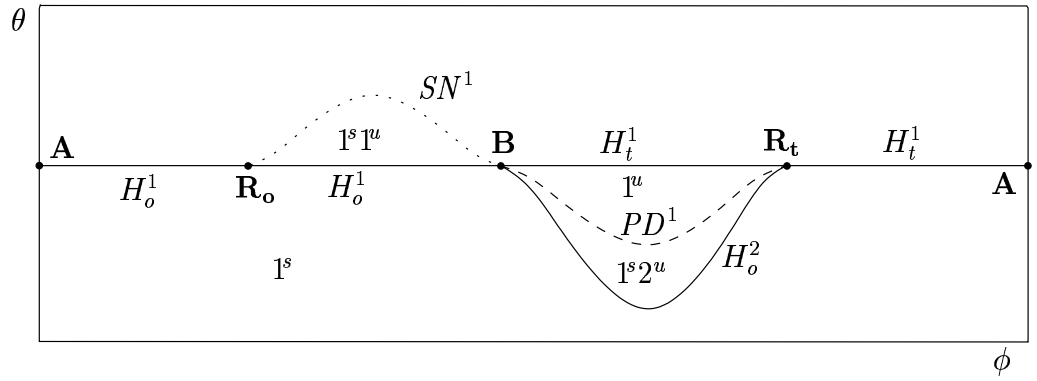

Figure 7. The conjectured unfolding for the transition from **A** to **B** in the "world map" representation given by (1). Note how this glues together the relevant codimension-two cases from Figures 4 and 6; see also Figure 8.

3. Sandstede's model

The model of Sandstede (1997) was explicitly constructed to contain codimension-two inclination and orbit flips for any eigenvalue configuration. This allows us to study the codimension-three case of a transition between two codimension-two homoclinic flip bifurcations of different type. We first introduce the model and then present the results of our numerical investigations.

Sandstede's model is given by the following set of equations:

$$\begin{aligned}
\dot{x} &= ax + by - ax^2 + (\tilde{\mu} - \alpha z)x(2 - 3x) + \delta z,\\
\dot{y} &= bx + ay - \frac{3}{2}bx^2 - \frac{3}{2}axy - (\tilde{\mu} - \alpha z)2y - \delta z,\\
\dot{z} &= cz + \mu x + \gamma xz + \alpha\beta(x^2(1 - x) - y^2).
\end{aligned} \tag{2}$$

Here $a, b, c, \mu, \tilde{\mu}, \alpha, \beta, \gamma$ and δ are parameters which take particular values at the different bifurcations. In the present context the parameter δ may be set to zero. The eigenvalues of the linearization at zero are then given by

$$\lambda_{1,2} = a \pm \sqrt{b^2 + 4\tilde{\mu}^2}, \quad \lambda_3 = c.$$

In this setting we take $|a| < b, 0 < b$ and $c < 0$. Then the following holds:

Theorem 1 (Sandstede (1997)) *A homoclinic solution of (2) contained in the Cartesian leaf, $\Gamma = \{(x, y, z) \mid x^2(1-x) - y^2 = 0,\ z = 0\}$ exists for $(\mu, \tilde{\mu}) = 0$. Furthermore, the following holds:*

(i) A resonant homoclinic bifurcation occurs for
$a = 0$ if $c < -\sqrt{b^2 + 4\tilde{\mu}^2}$ and for
$c = a + \sqrt{b^2 + 4\tilde{\mu}^2}$ otherwise. This bifurcation is unfolded by μ and a.

(ii) An inclination flip occurs for $c < a - b$ and $\beta = 1$. This homoclinic flip bifurcation is unfolded by the parameters μ and $\alpha - \alpha_0$ for a certain α_0 depending on a, b, c and γ. Moreover, in the unfolding the parameter μ breaks the homoclinic orbit and $\alpha - \alpha_0$ breaks the inclination flip on this orbit.

(iii) An orbit flip occurs for $c > a - b$, $\beta = 0$ and sufficiently small α, where $\alpha > 0$. In this case, the unfolding parameters are μ and $\tilde{\mu}$ and these are both involved in breaking the homoclinic orbit and the orbit flip on it.

An important aspect is that for $a = 0, b = 1, \mu = \tilde{\mu} = 0$ the explicit homoclinic solution is contained in the Cartesian leaf Γ and is given by an explicit expression

$$(x(t), y(t), z(t)) = (1 - \Big(\frac{1 - e^t}{1 + e^t}\Big)^2, 4e^t \frac{1 - e^t}{(1 + e^t)^3}, 0).$$

Using this solution as a starting point, the software HomCont (Doedel et al. 1997) can be used to trace curves of homoclinic orbits as parameters are varied.

4. The transition from A to B

This section treats the codimension-three bifurcations for which $\lambda_s = 1$, that is, where a transition from **A** to **B** takes place in Figure 5. For convenience we fix $\lambda_{ss} = 2$, so the central singularity has the stable eigenvalues $(\lambda_{ss}, \lambda_s) = (2, 1)$. We first handle the inclination flip and then the orbit flip.

Between the cases **A** and **B** there is a resonance. So for drawing a representation for this resonant flip bifurcation, one has to consider both types of resonant bifurcation together with the two codimension-two homoclinic flip bifurcations. The simplest way to connect them is sketched in our world map coordinates in Figure 7. The saddle-node curve originating at $\mathbf{R_o}$ connects to **B**, and the periodic-doubling and 2-homoclinic curves originating at this point connect to $\mathbf{R_t}$. The numerical investigations to be presented next were performed to see whether this proposed unfolding occurs in practice, or whether there is a more complicated structure.

4.1. From **A** *to* **B***; the inclination flip case*

As stated in Theorem 1(ii) for the inclination flip we can set $\tilde{\mu} = 0$. This simplifies the eigenvalues to $\lambda_1 = a - b$, $\lambda_2 = a + b$ and $\lambda_3 = c$. In the notation set up in Section 2,

the positive eigenvalue is scaled to 1. We can achieve this by setting $a+b=1$. Since $a-b>c$, we then have $\lambda_{ss}=-c=2$ and $\lambda_s=-(a-b)=-(2a-(a+b))=1-2a$.

The inclination flip is unfolded by $\alpha-\alpha_0$ for a certain value of α_0. As stated in Theorem 1, the homoclinic orbit exists for $\mu=0$, so μ unfolds the homoclinic bifurcation. We put the central singularity in parameter space at $(a,\mu,\alpha)=(0,0,\alpha_0)$ to unfold the resonant inclination flip in the transition from **A** to **B**. The parameter γ controls a normal form parameter in the various codimension-two bifurcations in such a way that the curves in the unfolding come closer or further apart when γ is varied. We set $\gamma=3$.

A suitable choice of α_0 can be found numerically by continuing a homoclinic orbit in HomCont in α and μ or $\tilde{\mu}$ (the latter remains zero), while fixing (a,b,c,γ) to be $(0,1,-2,3)$ at the resonance. HomCont is able to detect the inclination flip. We found, among other values, $\alpha_0\approx 0.2271891$, and used this value.

The set of unfolding coordinates which are used are

$$\begin{aligned}\nu_1&=1-\alpha/\alpha_0\\ \nu_2&=10\mu\\ \nu_3&=2a,\end{aligned}\tag{3}$$

such that in (ν_1,ν_2,ν_3)-space the central singularity is always at $(0,0,0)$.

Using the spherical coordinates (1), we obtained the numerical pictures in Figure 8. For $r=0.25$, the period-doubling and 2-homoclinic curves are carefully calculated (see below for details). The curves PD^1 and H^2_o go from **B** to $\mathbf{R_t}$, and the codimension-two sub-cases match with the unfoldings of Figures 4 and 6. However, for $r=0.25$ the saddle-node curve, which goes from $\mathbf{R_o}$ to **B**, is too close to the main homoclinic curve in parameter space so that we were unable to follow it. Hence, we are not able to depict it for $r=0.25$ and instead made a picture of it for $r=0.4$. Notice how, even at this value of r, the curve SN^1 is much closer to the curve H^1_o than the curves PD^1 and H^2_o are. This phenomenon is confirmed by the normal forms of the resonant homoclinic bifurcations given in Chow et al. (1990). These are exponentially flat curves, namely for some $a_0>1$ and $\phi_{\rm res}$ equal to the ϕ-value of the resonance

$$\theta=(\phi-\phi_{\rm res})\text{const}\ a_0^{-\frac{1}{|\phi-\phi_{\rm res}|}}$$

for the curve SN^1 versus

$$\theta=\text{const}\ a_0^{-\frac{1}{|\phi-\phi_{\rm res}|}}$$

for the curves PD^1 and H^2_o. At $r=0.4$, the curves PD^1 and H^2_o are involved in a much more complicated structure, which is why we did not draw these curves completely in this case. Here a clear trade-off is apparent between choosing the sphere too small and not being able to resolve curves that are approximately overlaid (the distance between them also depends exponentially on r) and choosing the sphere too large and incorporating a more complicated structure. Nevertheless, the two panels in Figure 8 taken together confirm that the unfolding is indeed as predicted and sketched in Figure 7.

The bifurcation diagram for $r=0.25$ was obtained as follows. The homoclinic orbit was followed in ϕ and θ, indeed obtaining the horizontal line $\{\theta=0\}$ up to numerical

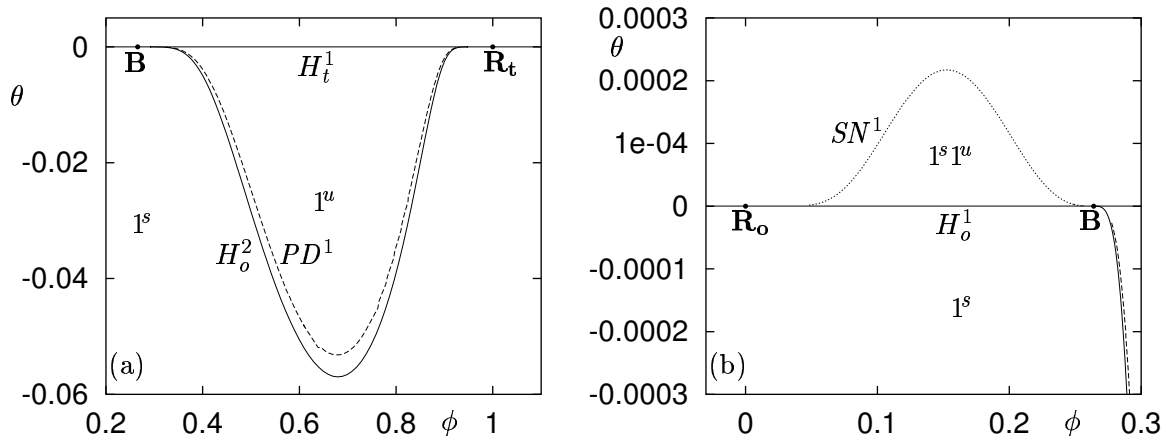

Figure 8. The numerically computed transition from **A** to **B** for the inclination flip for $r = 0.25$ (a) and $r = 0.4$ (b); compare Figure 7. Only period-doubling and homoclinic bifurcation curves can be seen in inset (a). In (b) only a small magnification near the curve H_o^1 is shown. A more complicated structure to the right of **B** was omitted. Notice the difference in scale between (a) and (b).

accuracy. At $\phi = 0.6$, the homoclinic orbit was then continued in the negative direction for the parameter θ as an unstable limit cycle. AUTO detected a period doubling bifurcation for $\theta = -0.04670363$. After that we switched onto the unstable period-doubled limit cycle and continued it again in θ. Doing so, the period grows to infinity as $\theta \to -0.05058922$, a clear sign that the 2-homoclinic orbit is being approached. We could switch to the 2-homoclinic orbit itself using a phase-shift routine which we implemented into HomCont; see Oldeman et al. (2000) for details. Both the period-doubling and 2-homoclinic bifurcation can then be continued in the two parameters Trying a similar technique to find the curve SN^1 was not successful due to its proximity to the curve H_o^1. However, for $r = 0.4$ we did succeed in finding and continuing the curve SN^1. At $\phi = 0.13$ the homoclinic orbit was continued in θ as an unstable limit cycle, which "bumps" into the saddle-node (a fold) at $\theta = 1.900846 \times 10^{-4}$ whereupon θ reverses its direction and a stable limit cycle is followed. This detected saddle-node bifurcation could be followed in two parameters using AUTO.

4.2. From **A** *to* **B***; the orbit flip case*

According to Theorem 1, when considering the orbit flip, we must have α not too large, $a - b < c$ and $\beta = 0$. Then the homoclinic orbit $q(t)$ of (2) undergoes a generic orbit-flip bifurcation with respect to the parameters $(\mu, \tilde{\mu})$. Since we want to have $\lambda_u = 1$ and $\lambda_{ss} = 2$ given $\nu_1 = 1 - \lambda_s$, and $a - b < c$ if $\tilde{\mu} = 0$, we have to choose a and b such that

$$\begin{aligned}\lambda_{ss} &= -(a - \sqrt{b^2 + 4\tilde{\mu}^2}) = 2,\\ \lambda_u &= a + \sqrt{b^2 + 4\tilde{\mu}^2} = 1,\\ \lambda_s &= -c.\end{aligned}$$

Now the unfolding parameters are

$$\begin{aligned} \nu_1 &= -\tilde{\mu}, \\ \nu_2 &= \mu, \\ \nu_3 &= 1 + c, \end{aligned} \tag{4}$$

such that the central singularity $(\nu_1, \nu_2, \nu_3) = (0, 0, 0)$ corresponds to $(\tilde{\mu}, \mu, c) = (0, 0, -1)$. Furthermore, we have set $\alpha = 1$ and $\gamma = 1$.

The transition has been investigated for different values of r, namely for $0.08, 0.1$ and 0.12. The numerical results for $r = 0.1$ are depicted in Figure 9. We see a more complicated figure here than for the inclination flip. The curves in this figure have been computed in the same way as for the inclination flip, but here we also found a Hopf-bifurcation, which was computed with AUTO by starting from the equilibrium point $(2/3, 0, 0)$ that exists for the parameter values $a = \mu = \alpha\beta = 0$. Observe that the limit cycles here end in this Hopf-bifurcation: they disappear by shrinking to a non-zero equilibrium.

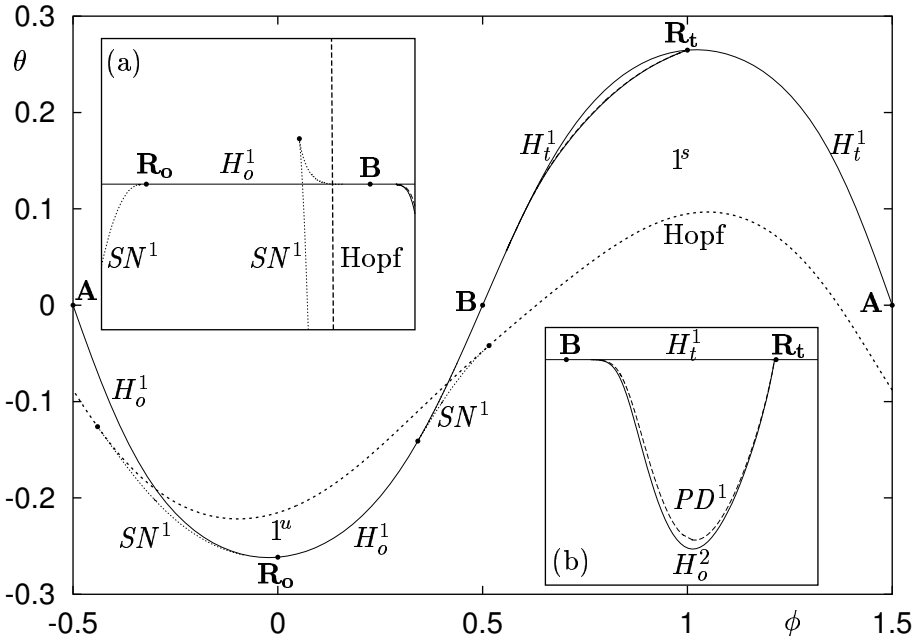

Figure 9. The transition from **A** to **B** for the orbit flip for $r = 0.1$. The insets show magnifications relative to the 1-homoclinic bifurcation-curve $H^1_{o/t}$. Inset (a) shows the cusp the curve SN^1 makes between the degenerate Hopf bifurcation and the point **B**. Inset (b) shows the curves PD^1 and H^2_o, which behave according to the theory.

Note that the saddle-node bifurcation curve originating at $\mathbf{R_o}$ does not go to **B** but ends in a degenerate Hopf (or Bautin) bifurcation (Kuznetsov 1998). The saddle-node curve originating at **B** also ends in a degenerate Hopf-bifurcation, but only after undergoing a cusp in between. Because this cusp is too close to be distinguished from the main homoclinic bifurcation the inset (a) shows a magnification of the location of

the saddle-node curve SN^1 relative to the main homoclinic curve H^1. This relative curve was obtained by subtracting the θ-values of the curve SN^1 from interpolated θ-values of the curve H^1. Similarly, in inset (b) we show the 2-homoclinic curve H^2_o and the period-doubling curve PD^1. These connect the points $\mathbf{B}$ and $\mathbf{R_t}$, as expected from the theory. So the picture is as predicted, apart from the Hopf, degenerate Hopf, and cusp bifurcations and the fact that there is no saddle-node curve connecting $\mathbf{B}$ and $\mathbf{R_o}$. Here a trade-off becomes apparent again, because, as explained below, for smaller values of r these bifurcations disappear from the sphere and the bifurcation diagram has the predicted form, although the curves in this diagram become extremely close to each other.

For the other values of r we present only pictures of the regions on the sphere that change qualitatively. In Figure 10, the bifurcation diagram for $r = 0.1$ is compared to the case $r = 0.08$. Figure 11 then shows some additional changes that take place near $\mathbf{R_t}$ as r is increased to 0.12.

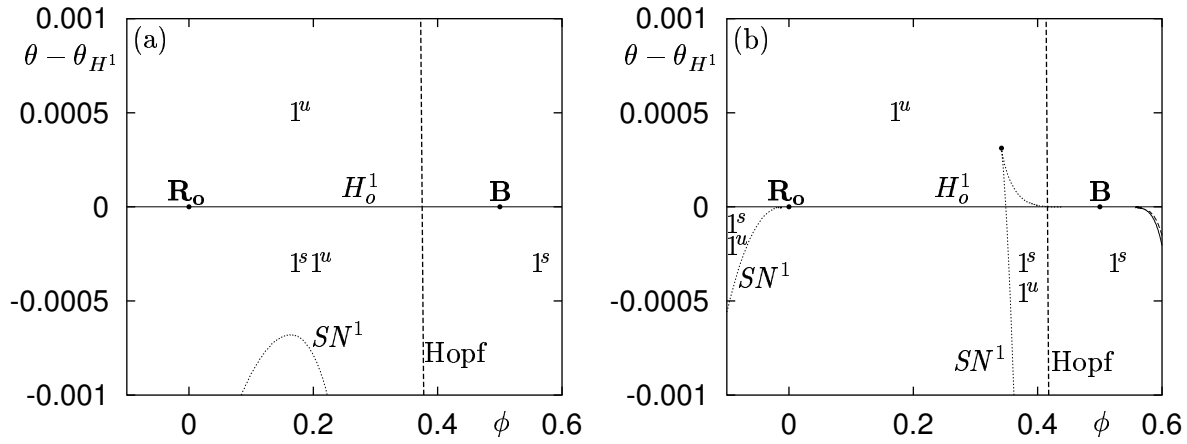

Figure 10. A comparison of the neighbourhood of $\mathbf{R_o}$ for $r = 0.08$ (a) and $r = 0.1$ (b), drawn relative to the curve H^1_o, showing the emergence of a cusp. Figure (b) is the same as inset (a) in Figure 9. Note that the scale of the two figures is exactly the same and that the curve SN^1 which connects the points $\mathbf{B}$ and $\mathbf{R_o}$ in panel (a) cannot be seen due to its proximity to the curve H^1_o.

If $r = 0.08$, the actual bifurcation diagram consists of a combination of the predicted bifurcation diagram in Figure 7 and a structure consisting of the Hopf-curve with two degenerate Hopf bifurcations connecting a curve SN^1. The latter structure is independent of the former, because its bifurcations occur at different areas of phase space. Indeed, numerically we found that for sufficiently small r, the Hopf-bifurcation structure is not on the sphere. This shows that the theory has been confirmed for the orbit flip as well, but for impractically small r.

If r is increased from 0.08 to 0.1, the following conjecture can be made. The saddle-node curve SN^1 touches the resonant point $\mathbf{R_o}$, and thereafter the left part of this curve remains connected to this point, whereas the right part forms a cusp with the SN curve

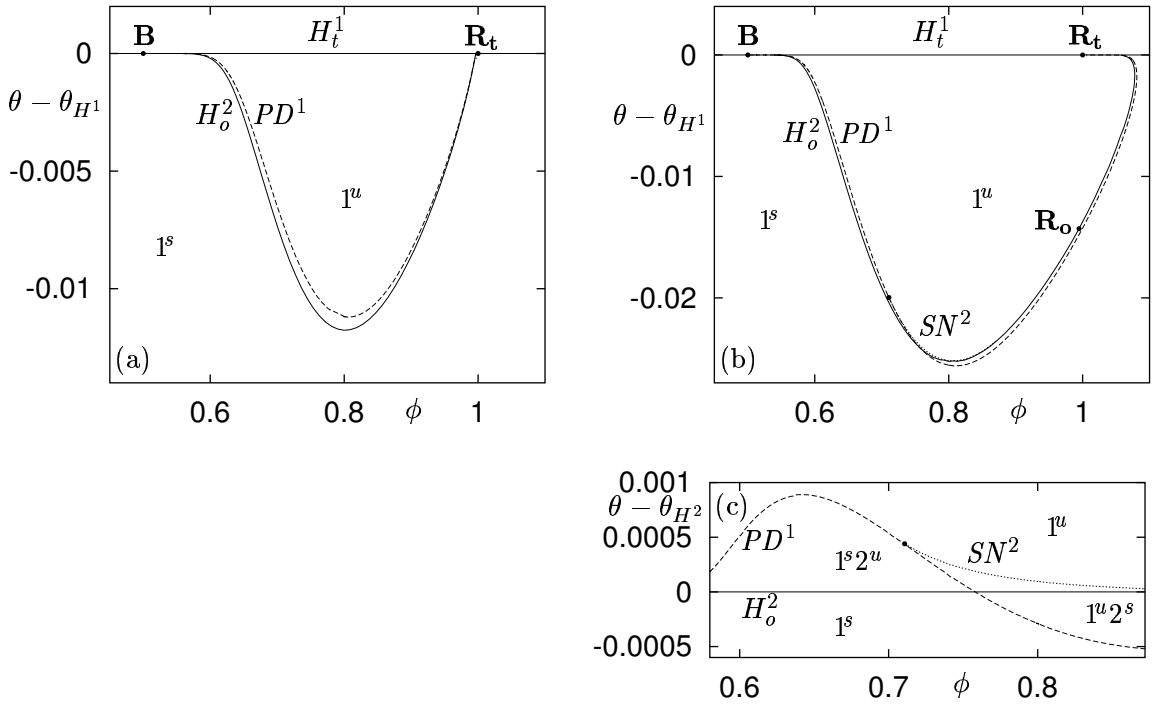

Figure 11. A comparison of the neighbourhood of $\mathbf{R_t}$ for $r = 0.1$ (a) and $r = 0.12$ (b) drawn relative to the curve H_o^1. The magnification (c) shows the curves PD^1 and SN^2 of (b) relative to the 2-homoclinic curve H_o^2. Figure (a) is the same as inset (b) in Figure 9. Note the difference by a factor of about 2 of the scales of panels (a) and (b), and the emergence of a curve SN^2 near the crossing of the curves PD^1 and H_o^2. These last two curves come in from a different direction at $\mathbf{R_t}$ in figure(b). The curve SN^2 goes from a degenerate period-doubling point on the curve PD^1 to a new point $\mathbf{R_o}$ on H_o^2.

originally going from $\mathbf{R_o}$ to $\mathbf{B}$. This process involves a codimension-three bifurcation, which occurs because a non-degeneracy condition in the codimension-two bifurcation $\mathbf{R_o}$ is not valid; see Chow et al. (1990). A conjectural unfolding of this bifurcation is shown in Figure 12(a) on a sphere, where we assume that this bifurcation also has cone structure. Note that the stability of the periodic orbits near the points $\mathbf{R_o}$ and $\mathbf{R_t}$ changes as well. These new types of resonant homoclinic bifurcations would have had $\eta_1 = \lambda_s - 1$ instead of $\eta_1 = 1 - \lambda_s$ in Figure 4.

Figure 11 shows that, between $r = 0.1$ and $r = 0.12$, the side on which the curves PD^1 and H_o^2 curves originate from the twisted resonance $\mathbf{R_t}$ changes. Because the curve H_o^2 then has to go through another resonance to arrive at $\mathbf{B}$, we see another side-switching bifurcation $\mathbf{R_o}$ here. The curve SN^2 originating from the new point $\mathbf{R_o}$ then connects to a degenerate period-doubling bifurcation point (see Figure 11(c)), which gives the possibility for the curves PD^1 and H_o^2 to cross each other independently. Thus the transition between the cases $r = 0.1$ and $r = 0.12$ involves another codimension-three bifurcation, coming from a violation of a non-degeneracy condition for the point

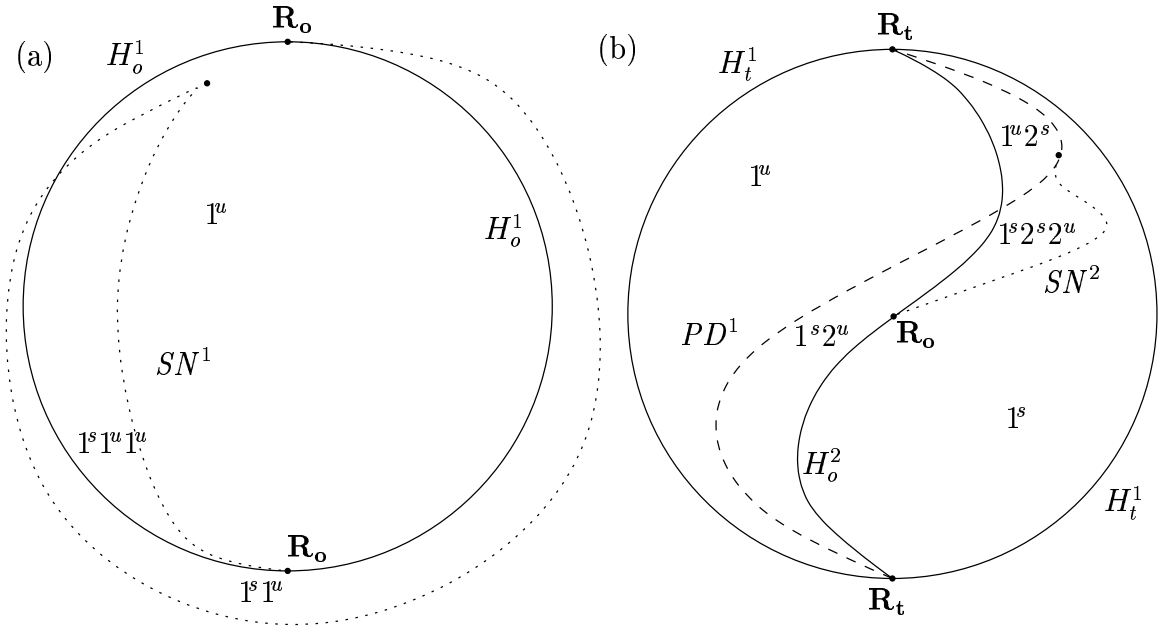

Figure 12. Conjectural unfoldings of degenerate resonant homoclinic bifurcations for the orientable (a) and the twisted (b) case. These unfoldings assume cone structure and are a representation on a sphere. They have the simplest possible structure to explain the phenomena occurring as r becomes larger in the numerical investigation of the resonant orbit flip bifurcation in Figures 10 and 11.

$\mathbf{R_t}$. A conjectural unfolding is depicted in Figure 12(b), again assuming cone structure.

A scenario not depicted here, and to be studied in detail elsewhere, is the following. As r becomes even larger, the homoclinic orbit appears to undergo a resonant inclination flip at $\mathbf{R_o}$. Then the resonance becomes twisted ($\mathbf{R_o}$ changes to $\mathbf{R_t}$) and new points **B** and **A** appear to the left and right of it, together with a curve SN^2 connecting **A** and $\mathbf{R_t}$, and curves PD^2 and H_o^4 that connect $\mathbf{R_t}$ and **B**. This new point $\mathbf{R_t}$ can then undergo another degenerate resonant homoclinic bifurcation. This process can repeat itself many times and this may be regarded as a mechanism for getting a partial "homoclinic-doubling cascade". A detailed exposition of this mechanism is left for future work. However, as we see in the next section, homoclinic-doubling cascades are an unavoidable part of the unfolding of the transition from **B** to **C**.

5. The transition from B to C

The central singularities we consider for this transition are both inclination flip and orbit flip bifurcations. Figure 5 depicts in the $(\lambda_s, \lambda_{ss})$-plane the location of the boundary between cases **B** and **C**. The resonant inclination flips we wish to address occur precisely on this boundary which has the two parts $\lambda_s = 1/2$ for $\lambda_{ss} > 1$ and $\lambda_{ss} = 1$ for $\lambda_s < 1$. The resonant orbit flips in question are at $\lambda_{ss} = 1$ for $0 < \lambda_s < 1$.

Contrary to the cases **A** and **B**, the bifurcation diagrams of the cases **B** and **C**

cannot be easily connected on a sphere. Recall that a codimension-three unfolding has these two points at opposite poles of the sphere, and hence we have to find a way to connect all the curves emanating from a point **C** to a point **B**. However, infinitely many curves emanate from **C** whereas only finitely many do from **B**. In particular, to complete the picture we therefore need a mechanism to generate higher-order homoclinic bifurcations.

One such mechanism is the *homoclinic-doubling cascade* (Homburg et al. 1997). It involves a sequence of inclination flips of type **B** for 2^n-homoclinic orbits. From each of these inclination flip bifurcation points a doubled homoclinic orbit emanates, and on this doubled orbit a new inclination flip occurs. The bifurcation diagram is made consistent by period-doubling and saddle-node bifurcation curves. It can be seen as a natural mechanism for the disappearance of a period-doubling cascade, in the sense that each of the limit cycles in the period-doubling cascade undergoes a homoclinic bifurcation and disappears (Oldeman et al. 2000). And just like for the period-doubling cascade, the homoclinic-doubling cascade is governed by scaling laws. However, contrary to the period-doubling cascade the scaling constants depend on the eigenvalues of the equilibrium; see also (Kokubu et al. 1996, Homburg and Young 1999).

In Homburg et al. (1997) it is explicitly proven that, given a certain open condition, a homoclinic-doubling cascade exists for the orbit flip case, where λ_{ss} is greater than but sufficiently close to 1 and $0.5 < \lambda_s < 1$. In Homburg and Krauskopf (2000) this result is extended to inclination flip bifurcations for eigenvalues in the region **B** close to the boundary with the region **C**. However, the precise structure of the bifurcation diagrams given in these articles remains conjectural.

In Oldeman et al. (2000) we investigated this homoclinic-doubling sequence of inclination flip bifurcations in detail, again via numerical computation on Sandstede's model, including justification of the scaling laws governing this cascade. We do not focus on the homoclinic-doubling cascade here, but we are interested in how it is embedded in the unfoldings of codimension-three resonant homoclinic flip bifurcations. Our numerical investigations to be presented next were performed to see whether the proposed unfoldings occur in practice.

5.1. From **B** *to* **C***; the inclination flip case*

For the inclination flip case, a transition from **B** to **C** can be made by crossing either of two different boundary curves. We consider both cases. The first one is the line $\lambda_s = 0.5$ for $\lambda_{ss} > 1$. In our numerical study we choose to fix $\lambda_{ss} = 2$, just as for the transition from **A** to **B** in Section 4. The second boundary is the line $\lambda_s = 1$ for $0.5 < \lambda_{ss} < 1$, where for the numerics we set $\lambda_{ss} = 0.75$.

5.1.1. Crossing $\lambda_s = 0.5$. To begin, we need to find parameters for a first inclination flip at $\lambda_s = 0.5$. We use the same parameters as in Section 4.1, except for those that change λ_s and α_0. The eigenvalue λ_s is now taken to be close to 0.5. We chose a suitable

value of α_0 for which this resonant inclination flip occurs, namely $\alpha_0 \approx 0.1222945$. Recall that we set $\lambda_{ss} = -c = 2$, which is the same as in Section 4.1.
The set of unfolding coordinates now are

$$\begin{aligned} \nu_1 &= 1 - \alpha/\alpha_0 \\ \nu_2 &= \mu \\ \nu_3 &= 1/2 - \lambda_s = 1/2 - (1 - 2a) = 2a - 1/2. \end{aligned} \tag{5}$$

We use the same technique for finding the 2-homoclinic curve as in Section 4. In order to compute 2^n-homoclinic orbits and associated period-doubling and saddle-node bifurcations, we repeat this process to find successively higher-order homoclinic orbits; for a more detailed explanation see Oldeman et al. (2000).

Figure 13 shows, in the spherical coordinates for the choice (5) of (ν_1, ν_2, ν_3), the numerical results we obtained in the (ϕ, θ)-plane for $r = 0.2$. Note that the 2-homoclinic curve $H^2_{o/t}$ emerging at $\mathbf{B_1}$ changes its orientation in the inclination flip bifurcation $\mathbf{B_2}$, and can be followed to $\mathbf{C}$. From $\mathbf{B_2}$ a 4-homoclinic curve $H^4_{o/t}$ emerges, changes its orientation in another inclination flip bifurcation, and can also be followed to $\mathbf{C}$, and so on. Hence, these numerical results show how each of the 2^n-homoclinic curves are created and then all end at the point $\mathbf{C}$.

In other words, by following H^2_o we encounter a homoclinic-doubling cascade. The panels of Figure 13 show subsequent magnifications which spell out its structure in detail. At each of the inclination flip points in the homoclinic-doubling cascade a period-doubling curve of the respective multiple of the basic period is created. The curve PD^1 starting at $\mathbf{B}$ can be continued to $\mathbf{C}$, and the same is true for the curves PD^2 and PD^4 emerging from the inclination flips of the homoclinic-doubling cascade. The saddle-node curve SN^1 starting at $\mathbf{B}$ continues through a cusp to $\mathbf{C}$. The saddle-node bifurcation curves (which are too small to be visible in Figure 13) emerging from the inclination flip points $\mathbf{B}$ of the homoclinic-doubling cascade connect to period-doubling curves PD^{2^n}, which then cross the curves $H^{2^{n+1}}_o$. These results confirm the unfolding for the conjectured transition from $\mathbf{B}$ to $\mathbf{C}$.

However, Figure 13 does not tell the complete story. The banana-shaped region between the homoclinic and the period-doubling curves contains complicated dynamics, which were also conjectured by Homburg and Krauskopf (2000), namely 'bubbles' of homoclinic-doubling cascades starting from an n-homoclinic orbit, where for instance $n = 3$ or $n = 5$. A bubble with base period three is depicted in Figure 14, together with two enlargements. Panels (a) and (b) show how the bubble is embedded in the banana-shaped region, whereas panel (c) shows the bubble on its own. We found this bubble by first locating a stable period-three orbit. This stable orbit exists in the tiny region between the curves SN^3 and PD^3. We were able to find it by a careful search in parameter space with the package DsTool (Back et al. 1992). After this orbit was found the numerical data defining the orbit was transferred to and continued in AUTO as a periodic orbit until it approached a homoclinic bifurcation. The 3-homoclinic orbit we found was then continued directly to obtain the curve $H^3_{o/t}$. Note that this 3-

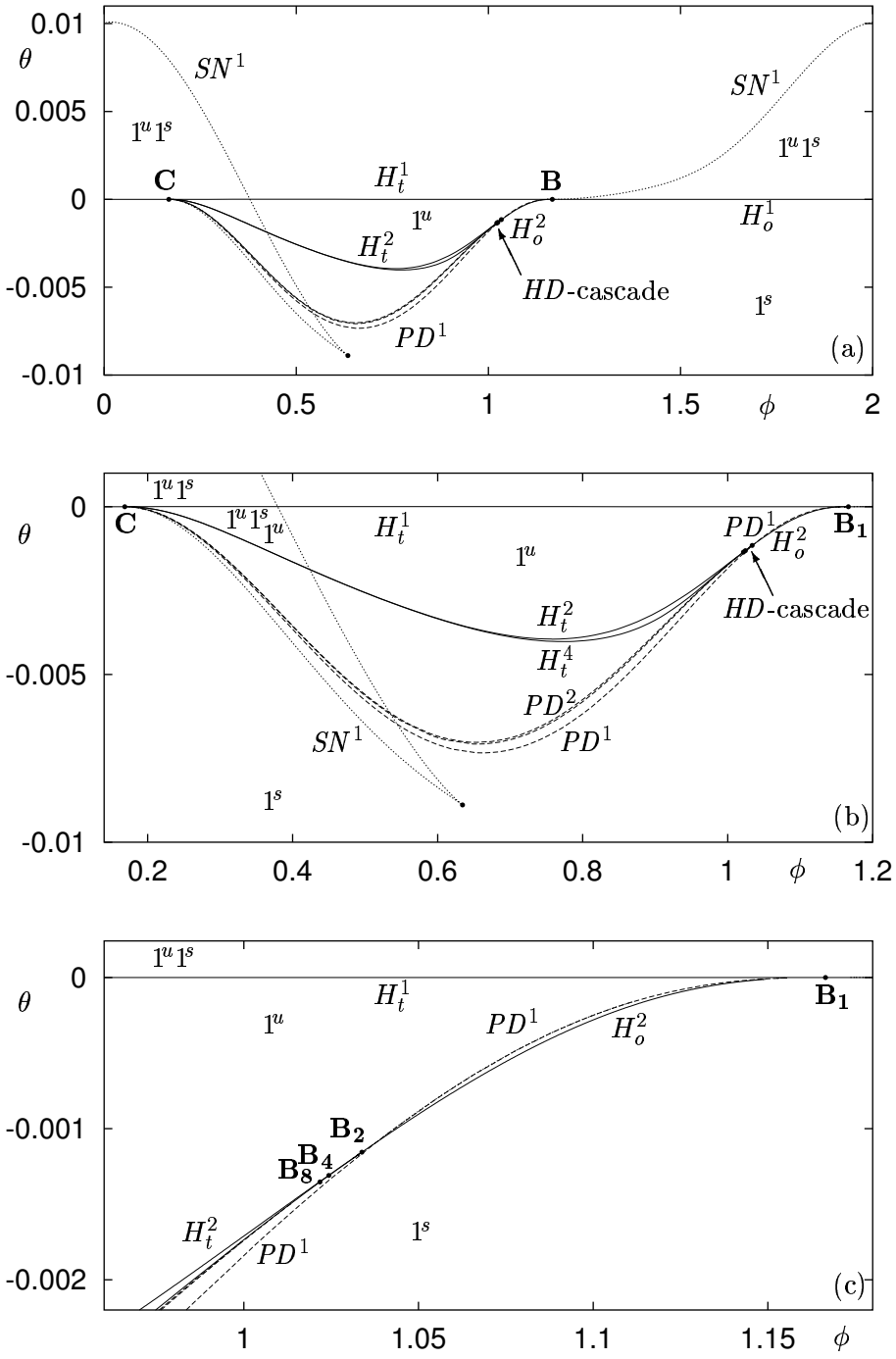

Figure 13. The numerically computed transition from **B** to **C** for the inclination flip involving a homoclinic-doubling cascade around $\lambda_{ss} = 2, \lambda_s = 0.5$. Panels (b) and (c) enlarge this cascade.

homoclinic orbit connects the primary inclination flip of type **C** to an order-3 inclination flip bifurcation also of type **C**; see Figure 14(c). This constitutes a bubble without a homoclinic-doubling cascade.

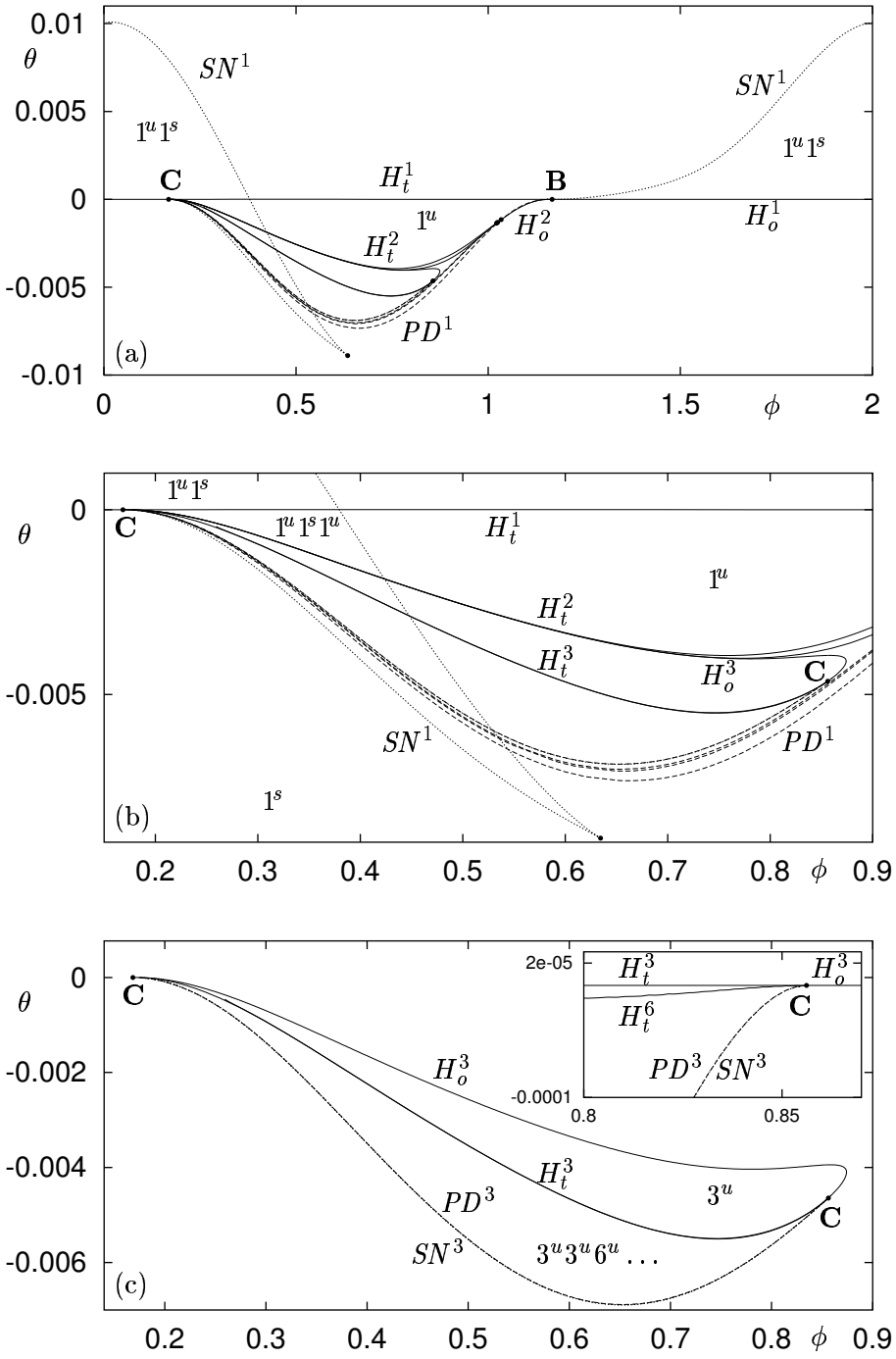

Figure 14. A base period-3 bubble in the computed transition from **B** to **C** for the inclination flip in Figure 13. Note that it does not involve a homoclinic-doubling cascade itself. Panel (a) gives an overview, panel (b) shows how the bubble is embedded in the main bifurcation diagram, and panel (c) shows it on its own, together with a magnification of the region around the point **C**.

However, by enlarging the sphere, as is shown in Figure 15, the base period-3

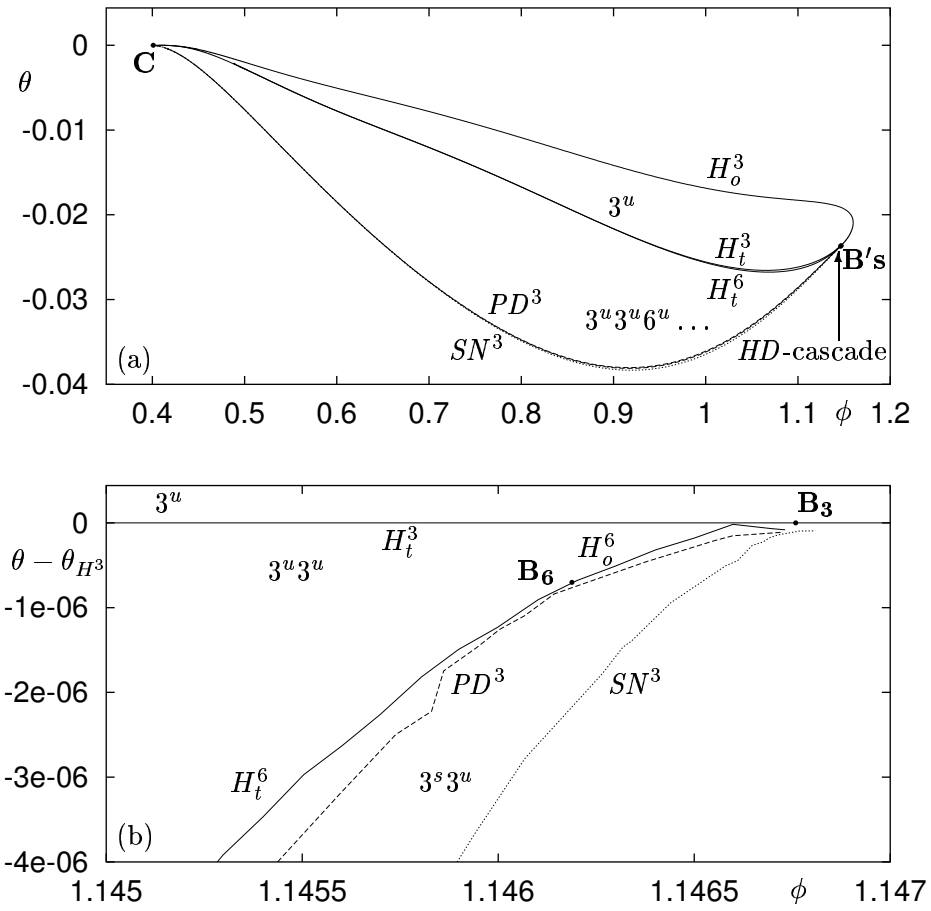

Figure 15. A bubble in the numerically computed transition from **B** to **C** for the inclination flip involving a homoclinic-doubling cascade, derived from the bubble in Figure 14. The sphere was made 1.5 times larger overall and an additional 5 times larger in the α-direction to obtain this bubble. The magnification (b) shows the structure of the homoclinic-doubling cascade on the bubble.

inclination flip of type **C** itself undergoes a resonant homoclinic flip bifurcation, as it is going through the boundary between **B** and **C**. Hence we obtain a full homoclinic-doubling cascade on the bubble. The enlargement in Figure 15(b) shows the structure of this cascade. Notice that we are approaching the limits of AUTO's accuracy. This cascade on the bubble, as conjectured, has the same structure as the main homoclinic doubling-cascade.

In the neighbourhood of inclination flips of type **C** there is also a chaotic region including horseshoe dynamics. Indeed, the existence of 3-periodic orbits on a generic period-doubling route to chaos provides an explanation for the existence of the 3-periodic and 3-homoclinic orbits occurring here.

5.1.2. Crossing $\lambda_{ss} = 1$. The second resonant inclination flip case involves crossing the boundary $\lambda_{ss} = 1$ for $0.5 < \lambda_s < 1$. For our numerical investigation we chose $\lambda_s = 0.75$ and set $a = 0.125$, $b = 0.875$, and $c = -1$ to achieve the desired eigenvalues $a + b = 1$, $a - b = -0.75$ and $c = -1$. A suitable inclination flip of the primary homoclinic orbit was found to occur for $\alpha_0 \approx 0.02688882$. The set of unfolding coordinates are then

$$\begin{aligned} \nu_1 &= 1 - \alpha/\alpha_0 \\ \nu_2 &= \mu \\ \nu_3 &= 1 - \lambda_{ss} = 1 + c. \end{aligned} \tag{6}$$

The results are depicted in Figure 16 and are broadly similar to those in Figure 13. Indeed we find a homoclinic-doubling cascade, as shown in the magnification (b), and this cascade has the same structure as the one in Figure 13. This is exactly what the theory predicts. However, note the smaller θ-scale, which makes the structure of the homoclinic-doubling cascade in inset (b) less clear because we are close to AUTO's accuracy limitations. Also note the different shape of period-doubling bifurcations. The way the saddle-node bifurcation curve SN^1 approaches the homoclinic flip bifurcation point **C** is different as well. We conjecture that there exists a cusp, like in Figure 13, but it is so close to **C** that we were unable to compute it.

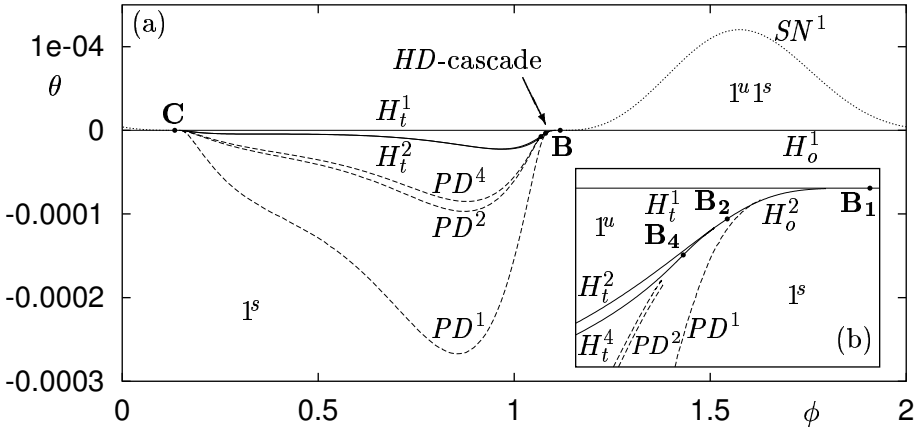

Figure 16. The numerically computed transition from **B** to **C** for the inclination flip involving a homoclinic-doubling cascade, around $\lambda_{ss} = 1, \lambda_s = 0.75$. The inset (b) shows a magnification of the homoclinic-doubling cascade.

These bifurcations constitute the main structure of the transition between **B** and **C**. We remark that other bifurcations are also present. We left them out for clarity in Figure 16 since they do not affect the main part of the bifurcation diagram. Nevertheless, we mention them here briefly for completeness. First, there is a torus bifurcation. It interferes with successive period-doubling bifurcations near the line defined by $\theta = -2 \times 10^{-5}$. In the process, the period-doubling bifurcations change from sub- to supercritical. The analysis of such an accumulation of "torus-doubling

bifurcations", which are codimension-two 1:2 resonant bifurcations and also give rise to more complicated dynamics, remains an open problem. It is worthy of study in its own right, and beyond the scope of this paper. An example of this phenomenon is described in (Kuznetsov 1998, end of Chapter 9).

The second additional phenomenon which does not seem to be connected with the central singularity is a different type of bubble. By continuing the bubble from the inclination flip case of Section 5.1.1, we could find a 3-homoclinic bubble here as well. However, this bubble seemed to be independent from the main bifurcation diagram and it lost its simple banana shape, cutting across the structure in Figure 16. Additionally it has a more complicated structure involving several additional folds and additional inclination flip points. Again, these features not directly relating to the unfolding of the transition from **B** to **C** will be investigated elsewhere.

5.2. From **B** *to* **C***; the orbit flip case*

The only boundary between regions **B** and **C** for the orbit flip is $\lambda_{ss} = 1$; see Figure 5. So at first glance there appears to be just one single case of a resonant orbit flip bifurcation between **B** and **C**. However, there are also two different cases here: $\lambda_s > 0.5$, involving a homoclinic-doubling cascade and $\lambda_s < 0.5$, not involving a homoclinic-doubling cascade. The reason for this is that all non-primary homoclinic flip bifurcations in the homoclinic-doubling cascade are inclination flips (Homburg et al. 1997) and those do not exist near the latter eigenvalue configuration; see again Figure 5. We consider both cases numerically, specifically taking $\lambda_s = 0.6$ and $\lambda_s = 0.49$.

We start by defining the parameters just like in Section 4.2. The difference is now that we want to have λ_{ss} close 1, and so a, b and c have to be such that

$$\begin{aligned}
\lambda_{ss} &= -(a - \sqrt{b^2 + 4\tilde{\mu}^2}) \approx 1, \\
\lambda_u &= a + \sqrt{b^2 + 4\tilde{\mu}^2} = 1, \\
\lambda_s &= -c = 0.6 \quad \text{or} \quad \lambda_s = -c = 0.49.
\end{aligned}$$

The coordinates (ν_1, ν_2, ν_3) corresponding to the spherical coordinates in (1) are now

$$\begin{aligned}
\nu_1 &= -\tilde{\mu} \\
\nu_2 &= -\mu \\
\nu_3 &= 1 - \lambda_{ss} = -(a - \sqrt{b^2 + 4\tilde{\mu}^2}) = 2a.
\end{aligned} \tag{7}$$

5.2.1. Crossing $\lambda_{ss} = 1$ for $\lambda_s > 0.5$. Figure 17 shows the numerical results in the (ϕ, θ)-plane for $r = 0.2$ and $\lambda_s = -c = 0.6$. A homoclinic-doubling cascade is clearly visible, just as it was for the inclination flips in Section 5.1. Note that the shape of the curve H_o^1 is similar to the one in the transition from **A** to **B** in Figure 9. The difference with the inclination flip figures is in the saddle-node curves SN^1: they interact with a Hopf bifurcation through degenerate Hopf (Bautin) bifurcations, much like in the transition from **A** to **B** for the orbit flip in Section 4.2. However, unlike in the transition

from **A** to **B**, at least for this value of λ_s, the interaction between the Hopf and the saddle node bifurcations does not seem to disappear if the sphere is made smaller. The theory by Homburg et al. (1997) indeed predicts that a homoclinic-doubling cascade should occur in this region, and the bifurcation diagram matches the conjectured one, except for the interaction with the Hopf bifurcation. This diagram is similar to the inclination flip diagrams because all non-primary homoclinic flip bifurcations are inclination flips. Remember that the common key feature of the orbit flip and the inclination flip is that in both cases the stable manifold changes its orientation; see also Nii (1996).

The banana-shaped region between the homoclinic and the period-doubling curves is also conjectured to contain "bubbles". These bubbles have the same structure as before, and hence we have left them out for brevity. Additionally, there is evidence of the existence of a torus bifurcation here, but for the same reasons as for the inclination flip case we do not depict it.

5.2.2. Crossing $\lambda_{ss} = 1$ for $\lambda_s < 0.5$. If λ_s is taken smaller than 0.5, the homoclinic-doubling cascade for the non-primary bifurcations collapse into one **C**-type inclination flip for the 2-homoclinic orbit. Figure 18 shows that for $\lambda_s = 0.49$ this is indeed the case. This figure is similar to Figure 17, except for the neighbourhood of the point **B**. In panel (a) the points **B** and $\mathbf{C_2}$ are so close together that we cannot distinguish them. Hence, a magnification is shown with respect to the curve H_o^2 in panel (b), in which we again reached the limits of AUTO's accuracy. Note that the period-doubling bifurcation curve PD^1 crosses the secondary homoclinic orbit H_t^2 after (to the left of) the **C**-type inclination flip. This crossing in itself is not a codimension-two bifurcation, but is like the crossing of the homoclinic and period-doubling bifurcation curves in the homoclinic-doubling cascade. The curve SN^2 emanating from the point $\mathbf{C_2}$ later on connects to the curve PD^1 in a degenerate period-doubling bifurcation. The curves PD^2 and H_o^4, emanating from $\mathbf{C_2}$, connect to the primary point **C** in panel (a). This is the case for all the curves of order 2^n that would also occur in the homoclinic-doubling cascade and emanate from $\mathbf{C_2}$. We did not investigate how all the other curves, such as the ones in bubbles, connect.

The part of the unfolding we computed confirm the proposed unfoldings. The fact that Figures 17 and 18 are so similar except for the region around the point **B** is interesting in its own right and is investigated next.

5.2.3. The transition through $\lambda_s = 0.5$. Figure 19(a) gives a representation of the situation near $\lambda_s = 0.5$. The purpose of this figure is to get a better understanding of what occurs when λ_s is varied, and we investigate how the 2-homoclinic inclination flip bifurcation, either $\mathbf{B_2}$ or $\mathbf{C_2}$, depends on the parameters λ_s and ϕ for several fixed values of r. It is a three-parameter continuation in λ_s, ϕ and θ, projected onto the (ϕ, λ_s)-plane. Since $\phi > 1$ corresponds to $\lambda_{ss} > 1$ in this part of the plane, the division of the regions **B** and **C** is exactly as in Figure 5.

For $\lambda_s < 0.5$ and $r = 0.2$ we see that there is only one inclination flip of type $\mathbf{C_2}$,

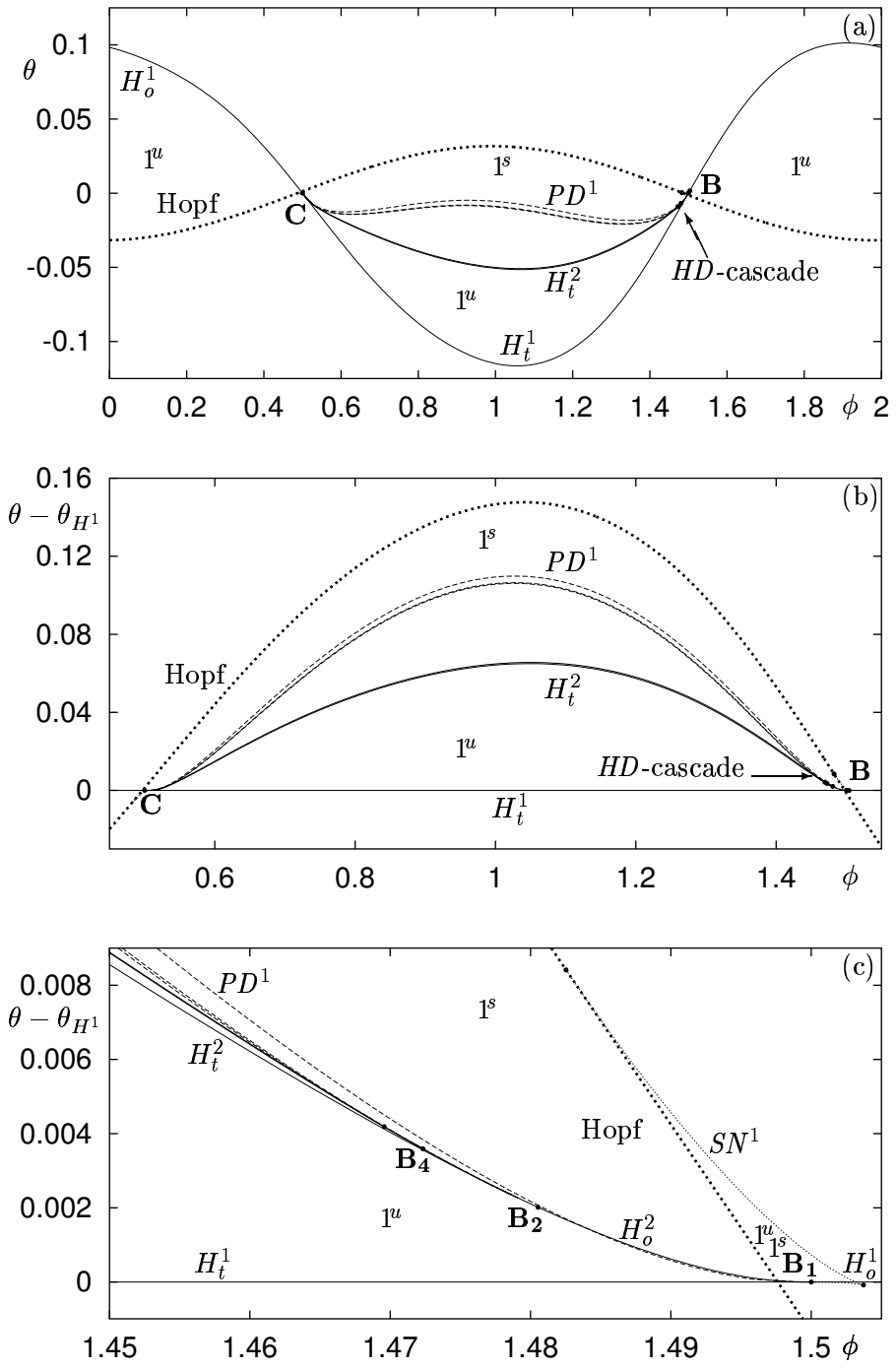

Figure 17. The numerically computed transition from **B** to **C** for the orbit flip involving a homoclinic-doubling cascade, around $\lambda_{ss} = 1, \lambda_s = 0.6$. Panels (b) and (c) show subsequent magnifications of the homoclinic-doubling cascade.

as shown in Figure 18. If $0.5 < \lambda_s < 0.61$, we see one inclination flip of type $\mathbf{B_2}$, which is the start of a homoclinic doubling cascade, as in Figure 17 and panel (c). However, if $\lambda_s > 0.62$, we have two additional inclination flips of type $\mathbf{C_2}$, as in the cross-section

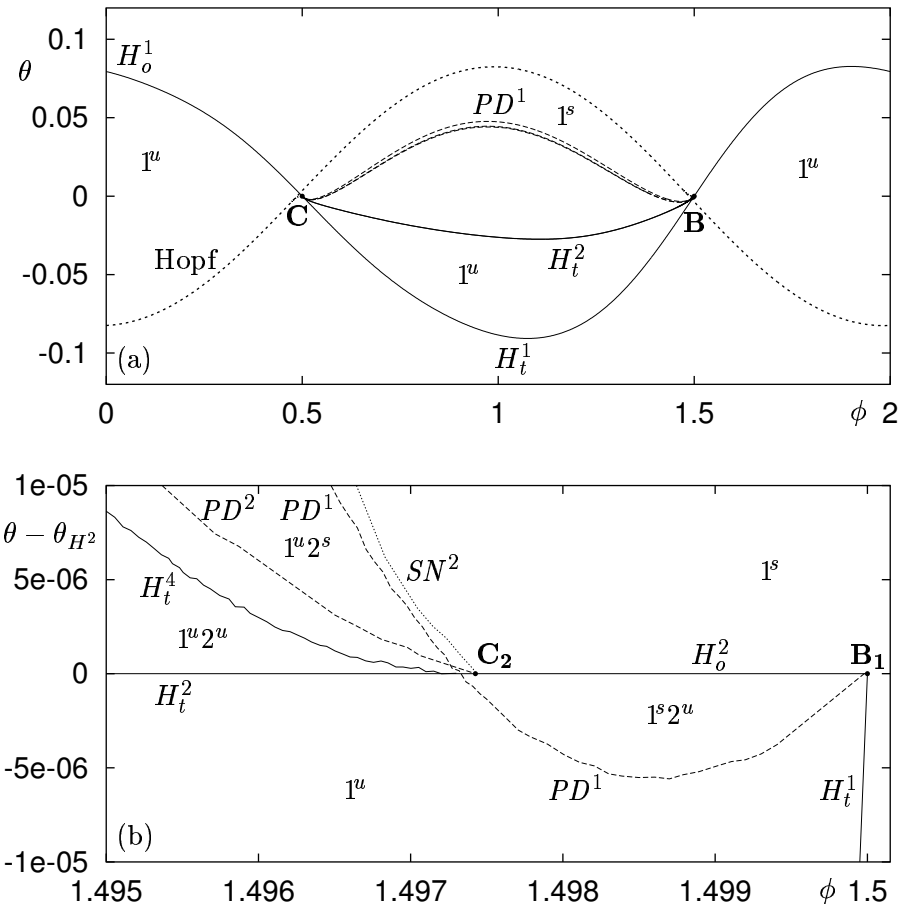

Figure 18. The numerically computed transition from **B** to **C** for the orbit flip *not* involving a homoclinic-doubling cascade, around $\lambda_{ss} = 1, \lambda_s = 0.49$. Panel (b) shows a magnification of the area around the point **B** relative to the curve H_o^2 (which does not exist to the right of $\mathbf{B_1}$). Note that only an inclination flip point $\mathbf{C_2}$ is present in this region, which spawns almost all the curves that connect to the primary point **C**.

panel (b). The bifurcation curves emanating from each of these points $\mathbf{C_2}$ are connected to each other in a highly complicated way. Successive inclination flips of type **C** appear to exist on branches of successively higher order homoclinic orbits with the net effect of producing a structure reminiscent of a homoclinic-doubling cascade. The particular details of this are yet unknown and beyond the scope of this paper. If we take λ_s even higher, but still less than 1, the inclination flip $\mathbf{B_2}$ disappears together with an inclination flip $\mathbf{C_2}$. Note that a homoclinic-doubling cascade cannot even exist then, which does not necessarily contradict the theorem of Homburg et al. (1997), because the extra open condition mentioned at the beginning of Section 5 may fail to hold. The other inclination flip $\mathbf{C_2}$ near $\theta = 0.5$ must still be present but we were unable to follow it up to $\lambda_s = 1$ due to numerical convergence errors.

Figure 18 also shows that the observed behaviour for $\lambda_s = 0.55$ changes if r is taken

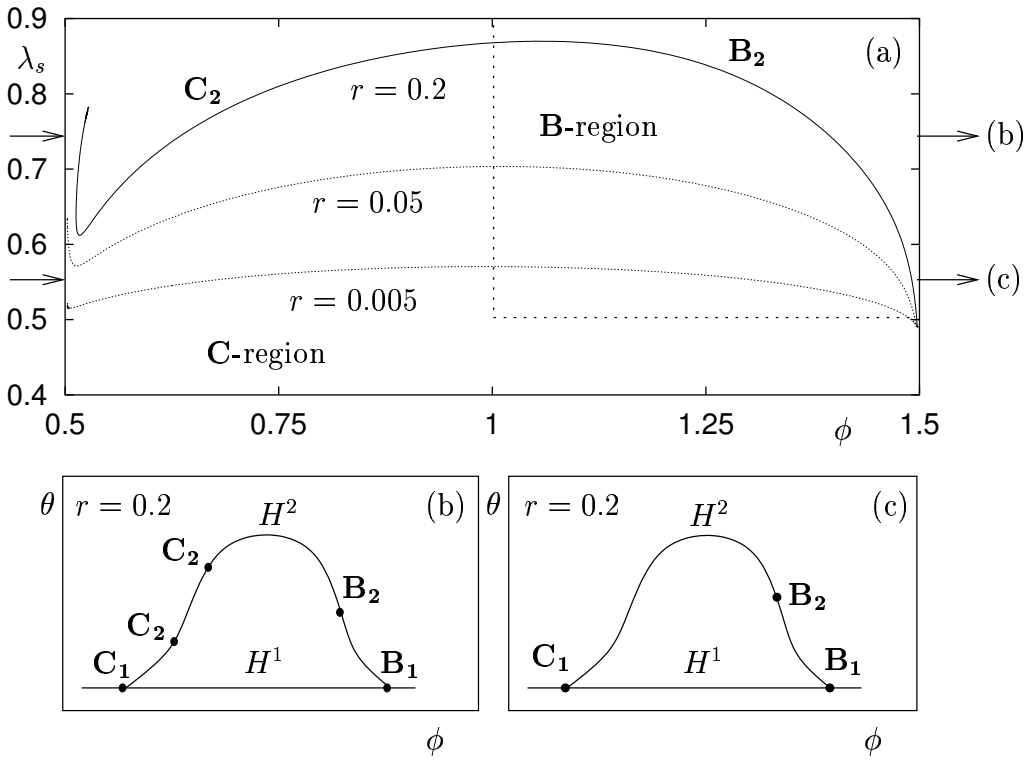

Figure 19. The behaviour of the resonant orbit flip changes as λ_s varies. Panel (a) shows a projection onto the (ϕ, λ_s)-plane of the locus of points at which the 2-homoclinic orbit undergoes an inclination flip of either type **B** or **C**. Three different values for the radius of the sphere are depicted, indicating qualitative differences. The **B** and **C** regions are divided by the dotted lines as shown. Note that for this range, $\phi > 1$ if and only if $\lambda_{ss} > 1$ (see also Figure 5). The panels (b) and (c) show two qualitative two-dimensional cross-sections as indicated in panel (a) for the values $\lambda_s = 0.75$ and 0.55 of curves in the (ϕ, θ)-plane for the solid curve $r = 0.2$.

smaller. If r is taken as small as 0.005, then the dotted line shows that the situation is like that for $r = 0.2$ and $\lambda_s = 0.9$. On the other hand, if we decrease λ_s to 0.51, we get the same bifurcation diagram back that we had for $r = 0.2$ and $\lambda_s = 0.55$. As we continue this process, we end up at $r = 0$ and $\lambda_s = 0.5$, so this situation hints at a complicated codimension-four point at this place first discussed by Homburg and Krauskopf (2000).

6. Conclusion

This is the first time that the various conjectured homoclinic codimension-three unfoldings have been checked in a numerical and global setting in a smooth vector field. Both the "simple" transition from **A** to **B** and the more complicated transition from **B** to **C** have been considered. For all possible sub-cases, the numerical investigations in this paper largely confirm the conjectural unfoldings by Homburg and Krauskopf

(2000) and indeed do appear to have cone structure. In this sense the present study is complete, although in the transition from **B** to **C** there remain unresolved issues, since the dynamics there involve infinitely many bifurcations of periodic orbits and artifacts like torus bifurcations and complex "bubbles".

The difficulty in the investigations for the simpler transition from **A** to **B** was mainly due to an important trade-off between finding bifurcation curves numerically and enlarging the sphere too much, in which case new codimension-three degenerate resonant homoclinic bifurcations were shown to appear. In Figure 12, conjectural unfoldings were given of these new bifurcations, based purely on numerical investigation. Moreover, one of them appears to contribute to a mechanism creating a partial homoclinic-doubling cascade. These bifurcations will be studied in more detail elsewhere.

The main difficulty in the transition from **B** to **C** was to unravel the complicated web of higher-order homoclinic bifurcations. This confirmed the conjectures to an astonishing degree, including the discovery of "bubbles" with and without homoclinic doubling cascades. The various fascinating mechanisms governing bifurcations which occur when changing the size of the sphere and the eigenvalues of the equilibrium bring out even more complicated behaviour. Indeed it appears that the dynamics involved in this model is infinitely rich. An example of extra dynamics is the phenomenon of accumulated 1:2 resonances due to a torus bifurcation curve interfering with a period-doubling cascade. It remains to be seen whether these phenomena occur universally in any model undergoing the codimension-three bifurcation in question, or are merely an artifact of Sandstede's model.

Especially for the transition from **B** to **C** involving a homoclinic-doubling cascade, it would be helpful to have a numerical method that switches directly from one homoclinic branch to another at a codimension-two point in parameter space. This would be a great improvement over the current indirect method which uses intermediate periodic orbits and a period-doubling bifurcation. Such a direct branch switching algorithm is currently under development.

How the unfoldings found here manifest themselves in models derived from physical applications, such as those mentioned in the introduction, remains an interesting topic for future research.

References

Back A, Guckenheimer J, Myers M, Wicklin F and Worfolk P 1992 Dstool: Computer assisted exploration of dynamical systems *Notices AMS* **39**(4), 303–309.

Champneys A R and Groves M D 1997 A global investigation of a solitary wave solutions to a fifth-order two-parameter model equation for water waves. *J. Fluid Mechanics* **342**, 199–229.

Champneys A R and Kuznetsov Y A 1994 Numerical detection and continuation of codimension-two homoclinic bifurcations *Int. J. Bifurcation and Chaos* **4**(4), 785–822.

Champneys A R, Kuznetsov Y A and Sandstede B 1996 A numerical toolbox for homoclinic bifurcation analysis *Int. J. Bifurcation and Chaos* **6**(5), 867–887.

Chow S N, Deng B and Fiedler B 1990 Homoclinic bifurcation at resonant eigenvalues *J. Dyn. Diff. Eqns.* **2**(2), 177–244.

Deng B 1989 The Shil'nikov problem, exponential expansion, strong λ-lemma, C^1-linearization, and homoclinic bifurcation *J. Diff. Eqns.* **79**, 189–231.

Deng B 1993 Homoclinic twisting bifurcations and cusp horseshoe maps *J. Dyn. Diff. Eqns.* **5**, 417–468.

Doedel E J, Champneys A R, Fairgrieve T F, Kuznetsov Y A, Sandstede B and Wang X 1997 *AUTO 97: Continuation and bifurcation software for ordinary differential equations (with HomCont).* `http://indy.cs.concordia.ca/auto`.

Evans J, Fenichel N and Feroe J A 1982 Double impulse solutions in nerve axon equations *SIAM J. Appl. Math.* **42**, 219–234.

Gaspard P, Arnéodo A, Kapral R and Sparrow C, eds 1993 *Homoclinic chaos* Vol. *Physica D 62 (Special Issue).*

Guckenheimer J and Holmes P 1983 *Nonlinear Oscillations, Dynamical Systems and Bifurcations of Vector Fields* Springer.

Homburg A J, Kokubu H and Naudot V 1997 Homoclinic doubling cascades. *Preprint* `http://www.math.uu.nl/people/homburg/cascade.ps.gz`.

Homburg A J and Krauskopf B 2000 Resonant homoclinic flip bifurcations. *To appear in J. Dyn. Diff. Eqns.* `http://www.math.uu.nl/people/homburg/homcod3_rev.ps.gz`.

Homburg A J and Young T 1999 Universal scalings in homoclinic doubling cascades. *Preprint* `http://www.math.uu.nl/people/homburg/homburg_99_renormalization.ps.gz`.

Kisaka M, Kokubu H and Oka H 1993*a* Bifurcations to N-homoclinic orbits and N-periodic orbits in vector fields *J. Dyn. Diff. Eqns.* **5**, 305–357.

Kisaka M, Kokubu H and Oka H 1993*b* Supplement to homoclinic-doubling bifurcation in vector fields *in* R Bamon, R Labarca, J Lewowicz and J Palis, eds *Dynamical Systems* Longman pp. 92–116.

Kokubu H, Komuru M and Oka H 1996 Multiple homoclinic bifurcations from orbit-flip. I. Successive homoclinic doublings *Int. J. Bifurcation and Chaos* **6**(5), 833–850.

Koper M 1995 Bifurcations of mixed-mode oscillations in a three-variable autonomous Van der Pol-Duffing model with a cross shaped phase diagram *Physica D* **80**, 72–94.

Krupa M, Sandstede B and Szmolyan P 1997 Fast and slow waves in the FitzHugh-Nagumo equation *J. Diff. Eqns.* **133**, 49–97.

Kuznetsov Y A 1998 *Elements of Applied Bifurcation Theory* 2nd edn (Springer).

Naudot V 1996 *Bifurcations Homoclines des Champes de Vecteurs en Dimension Trois* PhD thesis (l'Université de Bourgogne, Dijon).

Nii S 1996 N-homoclinic bifurcations for homoclinic orbits changing their twisting *J. Dyn. Diff. Eqns.* **8**, 549–572.

Oldeman B E, Krauskopf B and Champneys A R 2000 Death of period-doublings: locating the homoclinic-doubling cascade. *To appear in Physica D* `http://www.fen.bris.ac.uk/engmaths/research/reports/99r19.ps.gz`.

Rucklidge A M 1993 Chaos in a low-order model of magnetoconvection *Physica D* **62**, 323–337.

Sandstede B 1993 *Verzweigungstheorie homokliner Verdopplungen* PhD thesis Freie Universität Berlin, Institut für Angewandte Analysis und Stochastic. Report No. 7 (Berlin).

Sandstede B 1997 Constructing dynamical systems having homoclinic bifurcation points of codimension two *J. Dyn. Diff. Eqns.* **9**(2), 269–288.

Sandstede B 1999 Center manifolds for homoclinic solutions. *To appear in* J. Dyn. Diff. Eqns. `http://www.math.ohio-state.edu/~sandsted/Paper/center.ps.gz`.

Shashkov M V and Turaev D V 1999 An existence theorem of smooth nonlocal center manifolds for systems close to a system with a homoclinic loop *J. Nonlinear Sci.* **9**, 525–573.

Shil'nikov A L 1993 On bifurcations of the Lorenz attractor in the Shimizu-Morioka model *Physica D* **62**, 338–346.

Shil'nikov L P 1968 On the generation of periodic motion from trajectories doubly asymptotic to an equilibrium state of saddle type *Math. USSR Sb.* **6**, 427–437.

Shil'nikov L P 1969 On a new type of bifurcation of multidimensional dynamical systems *Sov. Math. Dokl.* **10**, 1368–1371.

Shil'nikov L P 1970 A contribution to the problem of the structure of an extended neighborhood of a rough equilibrium state of saddle-focus type *Math. USSR Sb.* **10**, 91–102.

Yanagida E 1987 Branching of double pulse solutions from single pulse solutions in nerve axon equations *J. Diff. Eqns.* **66**, 243–262.